

# A weighted Hybridizable Discontinuous Galerkin method for drift-diffusion problems \*

Wenyu Lei<sup>1</sup>, Stefano Piani<sup>1</sup>, Patricio Farrell<sup>2</sup>, Nella Rotundo<sup>3</sup>, and Luca Heltai<sup>1</sup>

<sup>1</sup>Mathematics Area, SISSA – International School for advanced studies, via Bonomea 265, 34136 Trieste, Italy

<sup>2</sup>Weierstrass Institute Berlin, Mohrenstr. 39, 10117 Berlin, Germany

<sup>3</sup>DIMAI – University of Florence, Viale Morgagni, 50127 Florence, Italy

November 7, 2022

## Abstract

In this work we propose a weighted hybridizable discontinuous Galerkin method (W-HDG) for drift-diffusion problems. By using specific exponential weights when computing the  $L^2$  product in each cell of the discretization, we are able to replicate the behavior of the Slotboom change of variables, and eliminate the drift term from the local matrix contributions. We show that the proposed numerical scheme is well-posed, and numerically validate that it has the same properties of classical HDG methods, including optimal convergence, and superconvergence of postprocessed solutions. For polynomial degree zero, dimension one, and vanishing HDG stabilization parameter, W-HDG coincides with the Scharfetter-Gummel stabilized finite volume scheme (i.e., it produces the same system matrix). The use of local exponential weights generalizes the Scharfetter-Gummel stabilization (the state-of-the-art for Finite Volume discretization of transport dominated problems) to arbitrary high order approximations.

**Keywords:** Finite element methods; discontinuous Galerkin methods; hybrid methods weighted norms; exponential fitting methods; convection-diffusion equations; drift-diffusion problems

---

\*This work was partially supported by funds from GNCS-INdAM “Professori Visitatori Bando 2020”, project “A comparison between Finite Volume and Hybridizable discontinuous Galerkin methods for the simulation of micro- and nano-electronic devices” as well as the Leibniz competition 2020.

# 1 Introduction

Drift-diffusion problems are ubiquitous in nature, and describe processes in which transport and diffusion play an equally important role. A notable example is the van Roosbroeck system for the simulation of the electric potential and charge carrier densities in semiconductor devices [25], where these systems are used to model the charge transport of electron or hole densities in a self-consistent electrical field.

Such systems are especially difficult to solve when advection dominates diffusion [26], leading to stiff boundary layers that need to be resolved appropriately by the numerical discretization schemes. Moreover, positivity preserving schemes are important when some of the unknown variables represent a density, as in the van Roosbroeck system.

The de-facto standard in the simulation of drift-diffusion problems is the finite volume method in combination with the Scharfetter–Gummel stabilization [29] — a finite volume variant of the Il’in–Allen–Southwell scheme [28].

Such scheme has become a key tool [17, 29, 5, 18, 10, 33] for the simulation of semiconductor devices, thanks to its positivity preserving property (cf. [6]), and to the availability of excellent mesh generators for complicated 2D [30] and 3D [31] domains, which allow to construct unstructured Delaunay–Voronoi meshes (though anisotropic meshes in 3D remain a challenge), capable of capturing boundary layers and other important features of the simulation.

One of the biggest drawback of the finite volume method is its inherent low order nature. An interesting attempt to construct uniformly convergent second order finite volume schemes for applications to semiconductor devices and plasma physics was undertaken by the group of ten Thije Boonkkamp. In a series of papers [20, 35, 36, 22], he and his coworkers have considerably extended a uniformly convergent second order finite difference scheme originally used by G. D. Thiart [34]. In [35], this approach was called *complete flux scheme* (CFS), owing to the fact that CFS has an additional source term contribution w.r.t. the well-known Scharfetter–Gummel flux of the differential operator.

This scheme was later extended to nonuniform meshes in [16], where also uniform second-order convergence was proven. However, it is not clear how to extend these ideas to produce finite volume schemes with convergence rates higher than two. Finite volumes, even when using Scharfetter–Gummel stabilization or the complete flux scheme, remain inherently low order methods.

Discontinuous Galerkin (DG) methods [4] are often thought to be a (possibly higher order) alternative to finite volume approximations, but are rarely adopted outside of the academic community. The combination of positivity preserving and the Scharfetter–Gummel stabilization makes the finite volume approximation very robust, and the *go-to* solution for many drift-diffusion approximations.

In this paper we propose a Weighted Hybrid Discontinuous Galerkin (W-HDG) method inspired by the construction of the complete flux scheme. In the Finite Volume context, CFS leads naturally to the Scharfetter–Gummel stabilization with some additional terms on the right hand side. When the

same idea is applied to HDG methods, one obtains a scheme that resembles exponential fitting methods [9, 8, 21], with some important differences.

W-HDG methods can be interpreted as a high order alternative to Scharfetter–Gummel Finite Volume discretizations. In Section 2 we introduce the problem, and the basic principles behind W-HDG methods. Section 3 presents some general notations common to all HDG discretizations, while Section 4 discusses stability, continuity, and convergence properties of the W-HDG method. We present some numerical examples and draw some conclusions in Sections 6 and 7.

## 2 Description of the problem

Given a function  $f$  defined on a bounded convex domain  $\Omega \subset \mathbb{R}^d$ , boundary data  $g_D$  and  $g_N$  respectively defined on  $\Gamma_D$  and  $\Gamma_N$ , where  $\Gamma_D \cup \Gamma_N = \Gamma := \partial\Omega$ , and  $\Gamma_D \cap \Gamma_N = \emptyset$ , we want to find the pair  $(u, \mathbf{j})$  satisfying

$$\mathbf{j} + \alpha \nabla u - \boldsymbol{\beta} u = 0, \quad \text{in } \Omega, \quad (1a)$$

$$\nabla \cdot \mathbf{j} = f, \quad \text{in } \Omega, \quad (1b)$$

$$u = g_D, \quad \text{on } \Gamma_D, \quad (1c)$$

$$\mathbf{j} \cdot \mathbf{n} = g_N, \quad \text{on } \Gamma_N. \quad (1d)$$

Here  $\mathbf{n}$  denotes the outward-pointing normal vector of  $\partial\Omega$ ,  $\alpha$  is assumed to be a positive constant, and the vector field  $\boldsymbol{\beta}$  is assumed to be in  $[L^\infty(\Omega)]^d$ .

When  $\mathbf{j}$  is kept as an independent variable as in system (1), the problem is in its mixed form (see, e.g., [7]). By substituting  $\mathbf{j}$  in equation (1b) with its definition in equation (1a) one obtains the classical primal formulation of the drift diffusion problem in divergence form.

If in addition the vector field  $\boldsymbol{\beta}$  is the gradient of a potential  $\psi$ , i.e.,  $\boldsymbol{\beta} = -\nabla\psi$ , one can rewrite both the primal and mixed formulation of the system using a change of variable

$$\mathbf{j} + \alpha \exp\left(-\frac{\psi}{\alpha}\right) \nabla s = 0, \quad \text{in } \Omega, \quad (2a)$$

$$\nabla \cdot \mathbf{j} = f, \quad \text{in } \Omega, \quad (2b)$$

$$s = g_D \exp\left(\frac{\psi}{\alpha}\right), \quad \text{on } \Gamma_D, \quad (2c)$$

$$\mathbf{j} \cdot \mathbf{n} = g_N, \quad \text{on } \Gamma_N. \quad (2d)$$

where the relation between  $u$  and  $s$  is given by

$$s = u \exp\left(\frac{\psi}{\alpha}\right), \quad (3)$$

and it is generally indicated as the Slotboom change of variables.

In system (1) the fluxes are split in drift and diffusive contributions, depending, respectively, on  $\boldsymbol{\beta}$  and  $\alpha$ . Rewriting system (1) using the set of variables

$(s, \mathbf{j})$  in place of  $(u, \mathbf{j})$ , has the effect of transforming the problem into a purely diffusive one, with a highly nonlinear coefficient  $\alpha \exp\left(-\frac{\psi}{\alpha}\right)$ .

The analysis of such problems flourished in the context of semiconductor devices, where a combination of nonlinear systems with a similar nature of system (1) describes the behavior of the electrostatic potential and charge transport. The most famous version of such problems – the van Roosbroeck system – involves three different variables: the electrostatic potential (with the same nature of  $\psi$ ), the electron density, and the hole density (both with the same nature of  $u$ ).

The rewriting of the van Roosbroeck system as a purely diffusive problem using the Slotboom change of variable (3) enabled the first analytical result with zero right-hand side in semiconductor theory [25], and was also used more generally in [23]. From the numerical point of view in [9] this set of variables was used to generalize the exponential fitting method to two-dimensional problems.

The Slotboom formulation has mostly analytical advantages, since it allows to write the system in terms of quasi-linear partial differential equations, and one can apply classical analytical results that can be found for example in [32] and used in the context of semiconductors coupled with circuits in [1] and [2].

One of the main difficulties in using directly the Slotboom formulation is the fact that the nonlinear diffusion coefficients remains treatable only when the ratio  $\frac{\psi}{\alpha}$  is of order one. In all other cases it rapidly blows up or goes to zero, rendering the numerical solution of the system difficult to deal with (see, e.g., [9]).

The idea behind our Weighted HDG formulation is to exploit a *local perturbation around the equilibrium* of the Slotboom transformation to eliminate the drift term from the system *element-wise*, as in equation (2a).

In order to have a mesh independent solution, we do not use directly the Slotboom variable  $s$ , but instead exploit weighted integrals to obtain the same effect of the Slotboom transformation, and we maintain the variable  $u$  as our system unknown.

Such formulation is possible by defining a locally shifted version of  $\psi$  which guarantees that  $\exp(\frac{\psi}{\alpha})$  is of order one in every element of the discretization, and using it as a weight in the integrals that define the local HDG systems (see Section 4 for the details).

### 3 Notation

In this section, we introduce some notations used to define our numerical scheme for the solution of problem (1).

#### 3.1 Subdivisions

Let us assume that the domain  $\Omega \subset \mathbb{R}^d$  is a polytope. Let  $\mathcal{T} := \mathcal{T}(\Omega)$  be a subdivision of  $\Omega$  made of simplices; we call the elements of  $\mathcal{T}$  “cells” and we call the intersection of two adjacent cells (or the intersection between a cell and  $\partial\Omega$ )

with positive  $(d-1)$ -measure a “face”. We denote with  $\mathcal{E}^\circ$  and  $\mathcal{E}^\partial$  the collection of these two kinds of faces and set  $\mathcal{E} := \mathcal{E}^\circ \cup \mathcal{E}^\partial$ . In what follows, we assume that  $\mathcal{T}$  is shape-regular in the sense of [15], i.e., there exists a positive constant  $c_1$  so that for each cell  $K \in \mathcal{T}$ ,

$$h_K \leq c_1 \rho_K,$$

where  $h_K$  is the size of  $K$  and  $\rho_K$  is the diameter of the largest ball inscribed in  $K$ .

### 3.2 Approximation spaces and jump operators

For  $K \in \mathcal{T}$ , we define  $\mathcal{P}_k(K)$  to be the space of polynomials defined on  $K$  with degree at most  $k$ . The vector space  $\mathcal{Q}(K) = [\mathcal{P}_k(K)]^d$  is used to approximate the flux  $\mathbf{j}$ , while the space  $\mathcal{W}(K) := \mathcal{P}_k(K)$  is used for approximating the scalar solution  $u$  in each element  $K$ . The corresponding global finite element spaces  $\mathcal{Q}(\mathcal{T})$  and  $\mathcal{W}(\mathcal{T})$  are respectively

$$\mathcal{Q}(\mathcal{T}) := \{\mathbf{Q} \in [L^2(\Omega)]^d : \mathbf{Q}|_K \in \mathcal{Q}(K)\}$$

and

$$\mathcal{W}(\mathcal{T}) := \{W \in L^2(\Omega) : W|_K \in \mathcal{W}(K)\}.$$

We note that the discontinuous functions  $\mathbf{Q} \in \mathcal{Q}(\mathcal{T})$  and  $w \in \mathcal{W}(K)$  are double valued when they are restricted to each interior face  $e \in \mathcal{E}^\circ$ . For two cells  $K^+, K^-$  such that  $e = K^+ \cap K^-$ , we define the branches  $W_{K^\pm}(\mathbf{x}) := \lim_{\epsilon \rightarrow 0} W(\mathbf{x} - \epsilon \mathbf{n}_{K^\pm})$  for all  $\mathbf{x} \in e$ , where  $\mathbf{n}_{K^\pm}$  denotes the outward normal vectors of  $K^\pm$ . The notation for the vector field  $\mathbf{Q}_{K^\pm}$  on  $e$  is similar. We also define the jump on  $e \in \mathcal{E}^\circ$ ,

$$[[W]]_e := W_{K^-} \cdot \mathbf{n}_{K^-} + W_{K^+} \cdot \mathbf{n}_{K^+} \quad \text{and} \quad [[\mathbf{Q}]]_e := \mathbf{Q}_{K^-} \cdot \mathbf{n}_{K^-} + \mathbf{Q}_{K^+} \cdot \mathbf{n}_{K^+}.$$

By convention, for  $e \in \mathcal{E}^\partial \cap K$  for some cell  $K$ , we define  $[[W]]_e = W_K \mathbf{n}_K$  and  $[[\mathbf{Q}]]_e = \mathbf{Q}_K \cdot \mathbf{n}_K$ .

For each face  $e \in \mathcal{E}$ , we similarly define  $\mathcal{M}(e) = \mathcal{P}_k(e)$  the polynomial space on  $e$  and

$$\mathcal{M}(\partial K) := \{\Lambda \in L^2(\mathcal{E}) : \Lambda|_e \in \mathcal{P}_k(e) \text{ for each face of } K\}.$$

The definition of the space  $\mathcal{M}(\mathcal{E})$  follows the same idea. Globally, we also define

$$\begin{aligned} \mathcal{M}_D(\mathcal{E}) := \{ & \Lambda \in L^2(\mathcal{E}) : \Lambda|_e \in \mathcal{P}_k(e) \\ & \text{for each } e \in \mathcal{E} \setminus \Gamma_D \text{ and } \Lambda|_e = G_D, \text{ for each } e \in \mathcal{E} \cap \Gamma_D\}, \end{aligned} \quad (4)$$

where  $G_D \in \mathcal{M}(\Gamma_D)$  is an approximation of  $g_D$  on  $\Gamma_D$ . In particular, we use the space  $\mathcal{M}_0(\mathcal{E})$  for  $\mathcal{M}_D(\mathcal{E})$  if  $G_D = 0$ .

### 3.3 Inner products and norms

For  $K \in \mathcal{T}$ ,  $e \in \mathcal{E}_K := \mathcal{E} \cap \partial K$ , and for a positive weight function  $\mu_K$  defined on  $K$ , we set

$$(u, v)_{K, \mu_K} := \int_K \mu_K uv \, d\mathbf{x} \quad \text{and} \quad \langle u, v \rangle_{e, \mu_K} := \int_e \mu_K uv \, ds_{\mathbf{x}},$$

and define the inner product  $\|\cdot\|_{K, \mu_K} = \sqrt{(\cdot, \cdot)_{K, \mu_K}}$ . We also set

$$\langle u, v \rangle_{\partial K, \mu_K} := \sum_{e \in \mathcal{E}_K} \int_e \mu_K uv \, ds_{\mathbf{x}}.$$

Globally, if  $\mu$  is defined as a cell-wise function so that  $\mu|_K = \mu_K$ , we introduce the weighted inner-product

$$(u, v)_{\mathcal{T}, \mu} := \sum_{K \in \mathcal{T}} (u, v)_{K, \mu}.$$

We set the norm  $\|\cdot\|_{\mu} := \sqrt{(\cdot, \cdot)_{\mathcal{T}, \mu}}$ . If the weight function  $\mu \equiv 1$  in  $\Omega$ , we omit the subscripts  $\mu$  or  $\mu_K$ .

## 4 Weighted HDG methods

In the section, we introduce our HDG method in the spirit of [13] assuming that  $\alpha$  is a positive constant, and that  $\beta$  is a piecewise constant function subordinate to a subdivision  $\mathcal{T}$  of  $\Omega$ . Then there exists a function  $\psi \in W^{1, \infty}(\mathcal{T})$  such that

$$\beta = -\nabla \psi \quad \text{locally on each } K. \quad (5)$$

Notice that, in general, the function  $\psi$  is not continuous across elements of  $\mathcal{T}$ .

### 4.1 Discrete formulation of the local problem

Let us start by considering problem (1) in a cell  $K \in \mathcal{T}$ . We multiply equation (1a) with a weight function

$$\mu_K(\mathbf{x}) := \exp\left(\frac{\psi(\mathbf{x})}{\alpha}\right) \quad (6)$$

satisfying that  $\nabla \mu_K = \frac{\nabla \psi}{\alpha} \mu_K = -\frac{\beta}{\alpha} \mu_K$ . Whence,

$$\mu_K \mathbf{j} + \alpha \nabla(\mu_K u) = 0, \quad \text{in } K \quad (7)$$

**Remark 1.** We note that the above equation would make sense globally (i.e., on the entire  $\Omega$ ) when  $\psi \in W^{1, \infty}(\Omega)$  and not just on each element separately. This assumption is satisfied, for example, by the Poisson equation for the electrostatic

potential  $\psi$  in the van Roosbroeck system. According to [23, Theorem 3.2.1], we can assume that the right hand side of the Poisson problem is in  $L^p(\Omega)$  if the doping concentration is assumed to be an  $L^p(\Omega)$  function with  $p > d$ . Whence by elliptic regularity  $\psi \in W^{2,p}(\Omega)$  (cf. [19, Theorem 4.3.2.2]) and we guarantee that  $\nabla\psi$  is Lipschitz by Sobolev embedding theorem.

Next, we test (7) with a vector-valued function  $\mathbf{Q} \in \mathcal{Q}(K)$  and multiply (1b) with  $\mu W$  where  $W \in \mathcal{W}(K)$ . Using integration by parts for the term containing  $\nabla(\mu_K u)$  and  $\nabla \cdot \mathbf{j}$ , our discrete weak formulation becomes: given a local Dirichlet boundary condition  $\widehat{U} \in \mathcal{M}(\partial K)$  and  $f \in L^2(K)$ , find  $(\mathbf{J}, U) \in \mathcal{Q}(K) \times \mathcal{W}(K)$  satisfying that for all  $\mathbf{Q} \in \mathcal{Q}(K)$  and  $W \in \mathcal{W}(K)$ ,

$$(\mathbf{J}, \mathbf{Q})_{K, \mu_K} - (\alpha U, \nabla \cdot \mathbf{Q})_{K, \mu_K} + \langle \alpha \widehat{U}, \mathbf{Q} \cdot \mathbf{n} \rangle_{\partial K, \mu_K} = 0, \quad (8a)$$

$$-(\mathbf{J}, \nabla W - \frac{\beta}{\alpha} W)_{K, \mu_K} + \langle \widehat{\mathbf{J}} \cdot \mathbf{n}, W \rangle_{\partial K, \mu_K} = (f, W)_{K, \mu_K}. \quad (8b)$$

Here the numerical flux  $\widehat{\mathbf{J}}$  is given by

$$\widehat{\mathbf{J}} = \mathbf{J} + \tau_K (U - \widehat{U}) \mathbf{n}, \quad (9)$$

with  $\tau_K \geq 0$  denoting a piecewise constant function (independent of  $h_K$ ) defined on  $\partial K$ .

**Remark 2** (Constant  $\beta$ ). *In particular, if  $\beta = -\nabla\psi$  is a constant vector, we shall use the following weight function*

$$\mu_K := \exp \left( - \frac{\beta \cdot (\mathbf{x} - \mathbf{x}_K)}{\alpha} \right), \quad (10)$$

where  $\{\mathbf{x}_K\}_{K \in \mathcal{T}}$  is a set of points in  $\mathbb{R}^d$ . As a consequence, the local problem (8) is rescaled by the factor  $\exp(-\beta \cdot \mathbf{x}_K / \alpha)$ . We will use the weight function (10) both for the analysis and for computational purposes by choosing different sets of  $\{\mathbf{x}_K\}$ ; see Section 4.6 and Section 6 for some particular choices.

The following proposition shows that the local problem admits a unique solution if the stabilization parameter is strictly positive on at least one face of  $K$ .

**Proposition 3** (Well-posedness of the local problem). *The local problem (8) is uniquely solvable if  $\tau_K \geq 0$  and it is strictly positive on at least one face of  $K$ .*

*Proof.* This proof follows closely [13, Proposition 3.2]. We report it here for completeness. It is sufficient to show that when  $\widehat{U} = 0$  on  $\partial K$  and  $f = 0$  in  $K$ , both  $\mathbf{J}$  and  $U = 0$  are trivial. To this end, we first apply integration by parts for the first term on the left hand side of (8b) and insert (9). Whence,

$$(\nabla \cdot \mathbf{J}, W)_{K, \mu_K} + \langle \tau_K (U - \widehat{U}), W \rangle_{\partial K, \mu_K} = 0. \quad (11)$$

We choose  $\mathbf{Q} = \mathbf{J} / \alpha$  in (8a) and  $W = U$  in (11) and sum up these two equations to get

$$\frac{1}{\alpha} (\mathbf{J}, \mathbf{J})_{K, \mu_K} + \langle \tau_K U, U \rangle_{\partial K, \mu_K} = 0. \quad (12)$$

Since  $\tau_K \geq 0$ , we immediately get  $\mathbf{J}_\Lambda = 0$  and  $\sqrt{\tau_K}U_\Lambda = 0$ . So  $\tau_K U_\Lambda = 0$ . By assumption,  $\tau_K$  is strictly positive at some face  $e$  of  $K$ . Then  $U = 0$  on  $e$ . If the polynomial degree  $k = 0$ , we get  $U = 0$  and the proof is complete. Otherwise, if  $k > 0$ , using the barycentric coordinate system, we can write  $U = l_e p_{k-1}$  with  $p_{k-1} \in \mathcal{P}_{k-1}(K)$  and where  $l_e$  is the corresponding barycentric coordinate function that vanishes on  $e$ . Since we have derived that  $\mathbf{J} = 0$ , according to (8a) with  $\mathbf{Q}$  satisfying  $\nabla \cdot \mathbf{Q} = p_{k-1}$  (this is because the divergence operator mapping from  $[\mathcal{P}_k(K)]^d$  to  $\mathcal{P}_{k-1}(K)$  is surjective), we have

$$0 = (\alpha U, p_{k-1})_{K, \mu_K} = \int_K \alpha \mu_K l_e p_{k-1}^2.$$

So  $p_{k-1} = 0$  and we conclude that  $U_\Lambda = 0$ .  $\square$

**Remark 4.** Proposition 3 implies that there exists a linear operator  $T$  mapping the data pair  $(\widehat{U}, f)$  to the solution pair  $(\mathbf{J}, U)$ .

## 4.2 Global system

At the continuous level, the global system (1) can be understood by combining the local system (7) and (1b) in each cell  $K$  and glue them together by the following transmission condition

$$[\![\mathbf{j}]\!]_e = 0, \quad \text{for all } e \in \mathcal{E}^\circ. \quad (13)$$

The boundary conditions follows from (1c) and (1d). Now for each face  $e \in \mathcal{E}$ , we shall impose (13), (1c) and (1d) weakly using the  $L^2(e)$  inner product as well as the discrete counterpart  $(\widehat{\mathbf{J}}, \widehat{U})$ . More precisely speaking, given the numerical flux  $\widehat{\mathbf{J}}$  defined by (9), for each face  $e \in \mathcal{E}^\circ$ ,

$$\langle [\![\widehat{\mathbf{J}}]\!], \xi \rangle = 0, \quad \text{for all } \xi \in \mathcal{M}(e) \quad (14)$$

and for each  $e \in \mathcal{E}^\partial$  and  $\xi \in \mathcal{M}(e)$ ,

$$\langle \widehat{U}, \xi \rangle_e = \langle g_D, \xi \rangle_e, \text{ if } e \in \Gamma_D \quad \text{and} \quad \langle \widehat{\mathbf{J}} \cdot \mathbf{n}, \xi \rangle_e = \langle g_N, \xi \rangle_e \text{ if } e \in \Gamma_N. \quad (15)$$

Noting that  $\widehat{U} = G_D := \pi g_D$  with  $\pi$  denoting the piecewise  $L^2$  projection on  $\Gamma_D(\mathcal{E})$ . We also observe that since  $[\![\widehat{\mathbf{J}}]\!] \in \mathcal{M}(e)$  and the formulation (14) immediately implies that  $[\![\widehat{\mathbf{J}}]\!] = 0$  on  $\mathcal{E}^\circ$ . Whence  $\widehat{\mathbf{J}}$  is single-valued on  $\mathcal{E}$ .

Our discrete formulation reads: find  $(\mathbf{J}, U, \widehat{U}) \in \mathcal{Q}(\mathcal{T}) \times \mathcal{W}(K) \times \mathcal{M}_D$  such that for all  $\mathbf{Q} \in \mathcal{Q}(\mathcal{T})$ ,  $W \in \mathcal{W}(\mathcal{T})$  and  $\xi \in \mathcal{M}_0(\mathcal{E})$ ,

$$\begin{aligned} (\mathbf{J}, \mathbf{Q})_{\mathcal{T}, \mu} - (\alpha U, \nabla \cdot \mathbf{Q})_{\mathcal{T}, \mu} + \sum_{K \in \mathcal{T}} \langle \alpha \widehat{U}, \mathbf{Q} \cdot \mathbf{n} \rangle_{\partial K, \mu} &= 0, \\ (\nabla \cdot \mathbf{J}, W)_{\mathcal{T}, \mu} + \sum_{K \in \mathcal{T}} \langle \tau_K (U - \widehat{U}), W \rangle_{\partial K, \mu} &= (f, W)_{\mathcal{T}, \mu}, \\ \sum_{K \in \mathcal{T}} \langle \mathbf{J} \cdot \mathbf{n} + \tau_K (U - \widehat{U}), \xi \rangle_{\partial K} &= \sum_{e \in \partial \Gamma_N} \langle g_N, \xi \rangle_e. \end{aligned} \quad (16)$$



### 4.3 Characterization of $\widehat{U}$

According to Remark 4,  $\mathbf{J}$  and  $U$  can be written as an operator acting on  $\widehat{U}$  and  $f$ . So when solving the discrete system (16), we can first eliminate the unknowns  $\mathbf{J}$  and  $U$  to rewrite the system only for  $\Lambda$ . In this subsection, we shall derive such system for  $\widehat{U}$  in order to investigate the well-posedness of (16). Using the notations from Remark 4, we denote the solution triplets

$$(\mathbf{J}_0, U_0, \widehat{\mathbf{J}}_0) \quad \text{and} \quad (\mathbf{J}_f, U_f, \widehat{\mathbf{J}}_f) \quad (17)$$

when  $f$  and  $g_D$  vanish respectively. More precisely, based on the discrete transmission condition (14) as well as the Neumann boundary condition defined in Equation (15), the solution  $\widehat{U} \in \mathcal{M}_D$  satisfies

$$a(\widehat{U}, \xi) = b(\xi), \quad \text{for all } \xi \in \mathcal{M}_0, \quad (18)$$

where

$$\begin{aligned} a(\widehat{U}, \xi) &= -\langle \llbracket \widehat{\mathbf{J}}_0 \rrbracket, \xi \rangle_{\mathcal{E}} \\ b(\xi) &= \langle \llbracket \widehat{\mathbf{J}}_f \rrbracket, \xi \rangle_{\mathcal{E}} - \langle g_N, \xi \rangle_{\Gamma_N} \end{aligned}$$

### 4.4 A decomposition of the bilinear form $a(.,.)$

Let  $\mu$  be a positive function defined in  $\Omega$  so that  $\mu|_K = \mu_K$  for every  $K \in \mathcal{T}$ . Then we decompose the bilinear form  $a(.,.)$  by

$$a(\widehat{U}, \xi) = \widetilde{a}(\widehat{U}, \xi) + E(\widehat{U}, \xi), \quad (19)$$

where

$$\widetilde{a}(\widehat{U}, \xi) = -\langle \llbracket \mu \widehat{\mathbf{J}}_0 \rrbracket, \xi \rangle_{\mathcal{E}} \quad \text{and} \quad E(\widehat{U}, \xi) = -(\langle \llbracket \widehat{\mathbf{J}}_0 \rrbracket, \xi \rangle_{\mathcal{E}} + \langle \llbracket \mu \widehat{\mathbf{J}}_0 \rrbracket, \xi \rangle_{\mathcal{E}}).$$

The following lemma provides a characterization of the bilinear form  $\widetilde{a}(.,.)$  assuming zero Dirichlet boundary condition.

**Lemma 5** (characterization of  $\widetilde{a}$ ). *The bilinear form  $\widetilde{a}(.,.)$  is symmetric semidefinite on  $\mathcal{M}_0 \times \mathcal{M}_0$ . Moreover, given any  $\Lambda \in \mathcal{M}_0$ , we denote  $(\mathbf{J}_\Lambda, U_\Lambda)$  the corresponding cell solutions by solving the local problem (8) with  $f = 0$  and recall (17). Then there holds that for  $\xi \in \mathcal{M}_0$ ,*

$$\widetilde{a}(\Lambda, \xi) = \frac{1}{\alpha} (\mathbf{J}_\xi, \mathbf{J}_\Lambda)_{\mathcal{T}, \mu} + \langle \llbracket \mu \tau (U_\Lambda - \Lambda) (U_\xi - \xi) \rrbracket, 1 \rangle_{\mathcal{E}} \quad (20)$$

where  $\tau$  is a function defined on  $\mathcal{E}$  so that  $\tau|_{\partial K} = \tau_K$ .

*Proof.* Before deriving (20), we first provide some essential identities. By summing up the local flux problem (8a) with  $\widehat{U} = \lambda$  for all  $K \in \mathcal{T}$ , we have

$$\frac{1}{\alpha} (\mathbf{J}_\Lambda, \mathbf{Q})_{\mathcal{T}, \mu} - (U_\Lambda, \nabla \cdot \mathbf{Q})_{\mathcal{T}, \mu} = -\langle \Lambda, \llbracket \mu \mathbf{Q} \rrbracket \rangle_{\mathcal{E}} \quad (21)$$

We use integration by parts for the first term on the left hand side of (8b) and sum up the equations for all  $K \in \mathcal{T}$  to obtain that (note that  $f = 0$ )

$$(\nabla \cdot \mathbf{J}_\Lambda, W)_{\mathcal{T}, \mu} = \langle \llbracket \mu(\mathbf{J}_\Lambda - \widehat{\mathbf{J}}_\Lambda)W \rrbracket, 1 \rangle_{\mathcal{E}}. \quad (22)$$

Using the above relations, we arrive at

$$\begin{aligned} \tilde{a}(\Lambda, \xi) &= -\langle \llbracket \mu \mathbf{J}_\Lambda \rrbracket, \xi \rangle_{\mathcal{E}} - \langle \llbracket \mu(\widehat{\mathbf{J}}_\Lambda - \mathbf{J}_\Lambda) \rrbracket, \xi \rangle_{\mathcal{E}} \\ &= \frac{1}{\alpha} (\mathbf{J}_\xi, \mathbf{J}_\Lambda)_{\mathcal{T}, \mu} - (U_\xi, \nabla \cdot \mathbf{J}_\Lambda)_{\mathcal{T}, \mu} \\ &\quad - \langle \llbracket \mu(\widehat{\mathbf{J}}_\Lambda - \mathbf{J}_\Lambda) \rrbracket, \xi \rangle_{\mathcal{E}} \quad \text{by (21) with } \Lambda = \xi, \mathbf{Q} = \mathbf{J}_\Lambda \\ &= \frac{1}{\alpha} (\mathbf{J}_\xi, \mathbf{J}_\Lambda)_{\mathcal{T}, \mu} + \langle \llbracket \mu(\widehat{\mathbf{J}}_\Lambda - \mathbf{J}_\Lambda)(U_\xi - \xi) \rrbracket, 1 \rangle_{\mathcal{E}} \quad \text{by (22) with } W = U_\xi. \end{aligned}$$

The proof is complete by inserting the definition of the numerical flux (9).  $\square$

**Remark 6.** *The above theorem also shows that the local problems (8) for all  $K \in \mathcal{T}$  together with the weak transmission condition*

$$\langle \llbracket \mu \widehat{\mathbf{J}} \rrbracket, \xi \rangle_{\mathcal{E}} = 0, \quad \text{for all } \xi \in \mathcal{M}_0.$$

*form a symmetric discrete system.*

**Remark 7.** *For  $\Lambda \in \mathcal{M}_0$ , we recall that*

$$0 \leq \tilde{a}(\Lambda, \Lambda) = \sum_{K \in \mathcal{T}} -\langle \widehat{\mathbf{J}}_\Lambda, \Lambda \rangle_{\partial K, \mu} =: \sum_{K \in \mathcal{T}} I_K.$$

*We can also show the above by proving the nonnegativity of  $I_K$ . Indeed, let  $\widehat{U} = \Lambda$ ,  $\mathbf{Q} = \mathbf{J}$  and  $W = U$  in (8) and sum up the equations with  $f = 0$  to derive that*

$$I_K = \frac{1}{\alpha} (\mathbf{J}_\Lambda, \mathbf{J}_\Lambda)_{K, \mu} + \langle \tau_K(U_\Lambda - \Lambda), U_\Lambda - \Lambda \rangle_{\partial K, \mu} \geq 0.$$

## 4.5 Well-posedness of the global problem (18) for constant $\beta$

Given a constant  $\beta$ , we choose  $\mathbf{x}_K$  to be the origin for all  $K \in \mathcal{T}$ . So the weight function  $\mu$  defined by (10) is continuous. Using this information, we can show that (18) is well-posed in the following theorem.

**Theorem 8.** *Assume that i)  $\psi$  is continuous and that  $\beta = -\nabla \psi$  is piecewise constant on  $\mathcal{T}$ , ii)  $\tau_K$  is positive on  $\partial K$  for all  $K \in \mathcal{T}$ . Then problem (18) is uniquely solvable.*

*Proof.* It suffices to show that given vanishing  $f$ ,  $g_D$ ,  $g_N$  such that  $a(\Lambda, \xi) = 0$  for all  $\xi \in \mathcal{M}_0$ , we can only obtain trivial solutions. Due to the continuity of the weight function  $\mu$  by choosing  $\mathbf{x}_K$  to be the origin and the fact that  $\widehat{\mathbf{J}}_\Lambda$  is single-valued, according to (19), we have  $E(\Lambda, \xi) = 0$  and hence  $0 = a(\Lambda, \xi) = \tilde{a}(\Lambda, \xi)$ .

Invoking Lemma 5 as well as Remark 7, we immediately obtain  $\mathbf{J}_\Lambda = 0$  in  $K$  and  $\tau_K(U_\Lambda - \Lambda) = 0$  on  $\partial K$ . By assumption for  $\tau_K$ ,  $\Lambda = U_\Lambda$  on  $\partial K$ . We next want to show that  $U_\Lambda = 0$ . Applying integration by parts in (8a) implies that

$$(\nabla(\mu U_\Lambda), \mathbf{Q})_K - \langle \mu(U_\Lambda - \Lambda), \mathbf{Q} \cdot \mathbf{n} \rangle_{\partial K} = 0. \quad (23)$$

We again apply  $U_\Lambda = \Lambda$  on  $\partial K$  into (23) to get

$$(\nabla(\mu U_\Lambda), \mathbf{Q})_K = 0, \quad \text{for all } \mathbf{Q} \in \mathcal{Q}(K). \quad (24)$$

Letting  $\mathbf{Q} = \nabla U_\Lambda - \frac{\beta}{\alpha} U_\Lambda \in \mathcal{Q}(K)$  implies that

$$0 = (\nabla(\mu U_\Lambda), \mathbf{Q})_K = (\nabla(\mu U_\Lambda), \nabla(\mu U_\Lambda))_{K,1/\mu}.$$

Hence, we deduce that  $U_\Lambda = C_K/\mu$  for some constant  $C_K$  in each  $K$  and  $\Lambda = U_\Lambda$  on  $\partial K$ . If  $\beta = 0$ , we derive that  $U_\Lambda$  is a constant and hence  $U_\Lambda = 0$  due to the vanishing Dirichlet boundary condition. If  $\beta \neq 0$ , as  $U_\Lambda \in \mathcal{W}(K)$ , we conclude that  $U_\Lambda = 0$  and hence  $\Lambda = 0$ . The proof is complete.  $\square$

**Remark 9.** *We can extend the above argument to show the well-posedness of the global system for the case when  $\beta = -\nabla\psi$  with  $\psi \in C^0(\Omega) \cap \mathcal{P}_1(\mathcal{T})$ . So  $\beta$  is a piecewise constant function and  $\mu$  is continuous. This will be used to develop the numerical scheme for drift-diffusion system when the electric potential  $\psi$  is approximated by continuous piecewise linear functions subordinate to  $\mathcal{T}$ .*

#### 4.6 Well-posedness for the one-dimensional case with $\beta \in L^\infty(\Omega)$

If  $\Omega = [a, b] \subset \mathbb{R}$ , we can further assume that  $\beta$  is a piecewise constant function even though  $\psi$  may not be continuous.

**Corollary 10.** *Assuming that  $\beta$  is a piecewise constant function with  $\beta_K := \beta|_K$ . We also assume that  $\tau_K$  is positive on  $\mathcal{E}$ . Then problem (18) is uniquely solvable.*

*Proof.* Our goal is to construct a continuous weight function  $\mu$  so that  $E(U_\Lambda, \xi) = 0$  in the proof of Theorem 8. We set  $\{\mathbf{x}_i\}_{i=0}^N$  are the grid points so that  $a = \mathbf{x}_0 < \dots < \mathbf{x}_N = b$  and set  $K_i = [\mathbf{x}_{i-1}, \mathbf{x}_i]$ . For each  $i = 1, \dots, N-1$ , we define  $\mu_{K_i}$  and  $\mu_{K_{i+1}}$  so that  $\mu$  is continuous at  $\mathbf{x}_i$ . To achieve this, we set

$$\frac{\beta_{K_i}}{\alpha}(\mathbf{x}_i - \mathbf{x}_{K_i}) = \frac{\beta_{K_{i+1}}}{\alpha}(\mathbf{x}_i - \mathbf{x}_{K_{i+1}}). \quad (25)$$

Given a fixed  $\mathbf{x}_{K_1} \in \mathbb{R}$ , we can solve for  $\mathbf{x}_{K_i}$  for  $i = 1, \dots, N$  based on (25) and hence the resulting  $\mu$  is continuous. The proof is complete according to the proof of Theorem 8.  $\square$

#### 4.7 Well-posedness for a general case

In this section we want to extend the assumption that there exists a function  $\psi \in W^{1,\infty}(\Omega)$  so that  $\beta = -\nabla\psi \in [L^\infty(\Omega)]^d$ . We then choose the weight function (6). To show the well-posedness of the global problem (18), we shall use the Poincaré inequality: for  $w \in H_D^1(\Omega)$ , there exists a constant  $C_p \sim C \text{diam}(\Omega)$  satisfying

$$\|w\|_{L^2(\Omega)} \leq C_p \|\nabla w\|_{L^2(\Omega)}.$$

**Theorem 11.** *Suppose that  $\psi \in W^{1,\infty}(\Omega)$ . We further assume that  $\|\beta\|_{L^\infty(\Omega)}$  is small enough such that the Poincaré constant satisfies*

$$\|\beta\|_{L^\infty(\Omega)} < \frac{2\alpha}{C_p} \quad (26)$$

*Under the assumption that  $\tau_K$  is positive on  $\partial K$  for all  $K \in \mathcal{T}$ , the discrete problem (18) is then uniquely solvable.*

*Proof.* Following the proof of Theorem 8, let us start our proof at (24). Under the current setting,  $\mathbf{Q} = \nabla U_\Lambda - \frac{\beta}{\alpha} U_\Lambda \notin \mathcal{Q}(K)$ . Here we choose  $\mathbf{Q} = \nabla U_\Lambda$ . We rewrite (24) to get

$$0 = (\nabla(\mu U_\Lambda), \nabla U)_K = \|\nabla(\mu^{1/2} U_\Lambda)\|_{L^2(K)}^2 - \left\| \frac{|\beta|}{2\alpha} \mu^{1/2} U_\Lambda \right\|_{L^2(K)}^2.$$

Now we sum up the above equation for all  $K \in \mathcal{T}$ . Note that  $U_\Lambda = \Lambda$  implies that  $U_\Lambda \in H_D^1(\Omega)$ . So  $\mu^{1/2} U_\Lambda \in H_D^1(\Omega)$ . By Poincaré inequality, we have

$$\begin{aligned} 0 &= \|\nabla(\mu^{1/2} U_\Lambda)\|_{L^2(\Omega)}^2 - \left\| \frac{|\beta|}{2\alpha} \mu^{1/2} U_\Lambda \right\|_{L^2(\Omega)}^2 \\ &\geq \left( \frac{1}{C_p^2} - \frac{\|\beta\|_{L^\infty(\Omega)}^2}{4\alpha^2} \right) \|\mu^{1/2} U_\Lambda\|_{L^2(\Omega)}^2. \end{aligned}$$

Assumption (26) shows that the constant on the right hand side above is strictly positive. Hence  $U_\Lambda = 0$  and the proof is complete.  $\square$

#### 4.8 A limiting case in the one-dimensional setting

Let us consider the numerical scheme (16) in 1d with  $k = 0$ , i.e., using piecewise constant functions. Set  $\Omega = (a, b)$  for some real numbers  $a < b$  and  $\Omega$  can be subdivided with  $a = \mathbf{x}_0 < \dots < \mathbf{x}_N = b$ . For  $i = 0, \dots, N-1$ , denote  $h_i = \mathbf{x}_{i+1} - \mathbf{x}_i$ . We also denote  $\{\Lambda_i\}_{i=0}^N$  the trace values on  $\mathbf{x}_i$  and  $\{(\mathbf{J}_i, U_i)\}_{i=1}^N$  the cell values on the interval  $(\mathbf{x}_{i-1}, \mathbf{x}_i)$ .

Using the constant test functions in (16), we can write  $\mathbf{J}_i$  as the function of  $\{\Lambda_i\}$ . That is for  $i = 1, \dots, N$ ,

$$\mathbf{J}_i = \frac{\alpha}{h_i} \left( B \left( \frac{\beta h_i}{\alpha} \right) \Lambda_{i-1} - B \left( -\frac{\beta h_i}{\alpha} \right) \Lambda_i \right), \quad (27)$$

where  $B(\cdot)$  is the Bernoulli function:

$$B(t) := \frac{t}{e^t - 1}.$$

The above flux is usually referred to as the Scherfetter-Gummel flux. For the second equation in (16), we write for  $i = 1, \dots, N$ ,

$$U_i = \frac{e_i \Lambda_{i-1} + e_{-i} \Lambda_i}{e_h + e_{-h}} + \frac{F_i}{\tau_i(e_i + e_{-i})} \quad (28)$$

with  $e_{\pm i} := \exp(\pm \frac{\beta h_i}{2\alpha})$  and  $F_i = \int_{\mathbf{x}_{i-1}}^{\mathbf{x}_i} f \mu$ . In terms of the discrete transmission condition, here we simply assume that the stabilization parameter  $\tau$  is a positive constant on  $\mathcal{E}$ . Under the piecewise constant setting, we write for  $i = 1, \dots, N-1$ ,

$$\mathbf{J}_i - \mathbf{J}_{i+1} + \tau(U_i + U_{i+1} - 2\Lambda_i) = 0. \quad (29)$$

Inserting (27) and (28) into (29) and letting  $\tau$  tend to zero to write the global problem for  $\Lambda$  by

$$\begin{aligned} & \frac{\alpha}{h_i} B\left(\frac{\beta h_i}{\alpha}\right) \Lambda_{i-1} \\ & - \left( \frac{\alpha}{h_i} B\left(-\frac{\beta h_i}{\alpha}\right) + \frac{\alpha}{h_{i+1}} B\left(\frac{\beta h_{i+1}}{\alpha}\right) \right) \Lambda_i \\ & + \frac{\alpha}{h_{i+1}} B\left(-\frac{\beta h_{i+1}}{\alpha}\right) \Lambda_{i+1} = F_i. \end{aligned} \quad (30)$$

The above system is identical to the system built using the finite volume method together with the Scherfetter-Gummel flux, justifying the interpretation of the W-HDG method as a high order generalization of the Scherfetter-Gummel stabilization.

## 5 Postprocessing

We propose two postprocessing procedures in an element-by-element fashion to obtain the density approximations of  $u$  using  $\mathcal{P}_{k+1}$  elements so that these approximations converges with order of  $O(h^{k+2})$  in both  $L^2(\Omega)$  and  $L^\infty(\Omega)$  norms.

### 5.1 Postprocessing by $L^2(K)$ minimization

We consider a density approximation  $U_* \in \mathcal{P}_{k+1}(\mathcal{T})$  so that for each  $K \in \mathcal{T}$ ,  $U_*$  minimize the functional

$$\int_K |\alpha \nabla U_* - \beta U + \mathbf{J}|^2 \, d\mathbf{x}$$

under the constraint  $\int_K (U_* - U) \, d\mathbf{x} = 0$ . We note that the constraint is necessary since  $U_* + C$  is also a minimizer of the above functional with  $C$  being any constant. The approximation  $U_*$  can be obtained by solving the following local problem:

$$\begin{aligned} (1, U_*)_K &= (1, U)_K, \\ (\alpha \nabla U_*, \nabla W) &= (\beta U - \mathbf{J}, \nabla W), \quad \text{for all } W \in \mathcal{P}_{k+1}(K). \end{aligned} \quad (31)$$

We note that  $U_*$  has a superconvergence property with rate  $O(h^{k+2})$  in the  $L^2(\Omega)$ -sense since both  $U$  and  $\mathbf{J}$  converge in optimal rate  $O(h^{k+1})$  and the local average of  $U$ , i.e.,  $\frac{1}{|K|} \int_K U$  super converges at rate  $O(h^{k+2})$  (cf. [14]). The numerical simulation provided in Section 6 also suggests that if  $u$  is smooth enough, the postprocess approximation also converges in  $L^\infty(\Omega)$  with rate  $O(h^{k+2})$ . We also need to point out that this postprocessing results does not satisfy the local problem (8) in any sense.

## 5.2 Postprocessing based on the local problem (8)

We next construct an postprocessing approximation based on the local problem (8) following the idea from [27]. The procedure needs more computations compared to the  $L^2(K)$ -minimization.

### 5.2.1 Reconstruction for the flux

We shall first reconstruct the flux approximation  $\mathbf{J}$  in the space  $H(\text{div}, \Omega)$ , the vector space in  $[L^2(\Omega)]^d$  so that its divergence belongs to  $L^2(\Omega)$ . To achieve this, we consider the piecewise Raviart-Thomas-Nédélec space  $\mathcal{RTN}_k(\mathcal{T}) = \{\mathbf{Q} \in [L^2(\Omega)]^d : \mathbf{Q}|_K \in \mathcal{RTN}_k(K)\}$ , where  $\mathcal{RTN}_k(K) := [\mathcal{P}_k(K)]^d + \mathbf{xP}(K)$ . Using the cell approximation  $\mathbf{J}$  as well as the trace approximation  $\widehat{\mathbf{J}}$ , we define the reconstruction  $\mathbf{J}_{div} \in \mathcal{RTN}_k(\mathcal{T})$  as

$$\begin{aligned} \langle \mathbf{J}_{div} \cdot \mathbf{n}, \mathbf{Q} \rangle_e &= \langle \mathbf{J} \cdot \mathbf{n}, \xi \rangle_{\partial K}, \quad \text{for all } \xi \in \mathcal{P}_k(e), \\ (\mathbf{J}_{div}, \mathbf{Q})_K &= (\widehat{\mathbf{J}}, \mathbf{Q})_K, \quad \text{for all } \mathbf{Q} \in [\mathcal{P}_{k-1}(K)]^d \text{ if } k \geq 1. \end{aligned} \quad (32)$$

Here we have to point out some properties of  $\mathbf{J}_{div}$ : (1) since  $\widehat{\mathbf{J}}$  is single valued on  $\mathcal{E}$ , the normal component of  $\mathbf{J}_{div}$  is continuous across interior faces. So  $\mathbf{J}_{div} \in H(\text{div}, \Omega)$ ; (2) [12] shows that both  $\mathbf{J}_{div}$  and  $\nabla \cdot \mathbf{J}_{div}$  converge in optimal rate  $O(h^{k+1})$ , which is crucial to the postprocessing of  $u$  in the next step.

### 5.2.2 Postprocessing of $U$

Our reconstruction of  $U$  is based on the problem (1) defined on each element  $K$  together with a Neumann boundary condition, i.e., at the continuous level, we want to find the pair  $(\mathbf{j}^*, u^*)$  satisfying

$$\begin{aligned} \mathbf{j}^* + \alpha \nabla u^* - \beta u^* &= 0, & \text{in } K, \\ \nabla \cdot \mathbf{j}^* &= \nabla \cdot \mathbf{J}_{div}, & \text{in } K, \\ \mathbf{j}^* \cdot \mathbf{n} &= \mathbf{J}_{div} \cdot \mathbf{n}, & \text{on } \partial K. \end{aligned}$$

Similar to the  $L^2(K)$  minimization scheme, we also need the constraint  $\int_K(u^* - U) = 0$  to guarantee that the local reconstruction is unique.

Now we are ready to define an approximation of  $(\mathbf{j}^*, u^*)$  by modifying the discrete local problem (8): letting  $\mathcal{Q}^*(K)$ ,  $W^*(K)$  and  $\mathcal{M}^*(\partial K)$  be the polynomial spaces like  $\mathcal{Q}(K)$ ,  $W(K)$  and  $\mathcal{M}(\partial K)$  but with the degree  $k+1$ , we want to find  $(\mathbf{J}^*, U^*, \hat{U}^*) \in \mathcal{Q}^*(K) \times W^*(K) \times \mathcal{M}^*(\partial K)$  such that  $\int_K(U^* - U) = 0$  and for all  $\mathbf{Q} \in \mathcal{Q}^*(K)$ ,  $W \in W^*(K)$  and  $\xi \in \mathcal{M}^*(K)$ ,

$$\begin{aligned} (\mathbf{J}^*, \mathbf{Q})_{K, \mu_K} - (\alpha U^*, \nabla \cdot \mathbf{Q})_{K, \mu_K} + \langle \alpha \hat{U}^*, \mathbf{Q} \cdot \mathbf{n} \rangle_{\partial K, \mu_K} &= 0, \\ -(\mathbf{J}^*, \nabla W - \frac{\beta}{\alpha} W)_{K, \mu_K} + \langle \hat{\mathbf{J}}^* \cdot \mathbf{n}, W \rangle_{\partial K, \mu_K} &= (\nabla \cdot \mathbf{J}_{div}, W)_{K, \mu_K}, \\ \langle \hat{\mathbf{J}}^* \cdot \mathbf{n}, \xi \rangle_{\partial K} &= \langle \mathbf{J}_{div} \cdot \mathbf{n}, \xi \rangle_{\partial K}, \end{aligned} \quad (33)$$

with the numerical flux  $\hat{\mathbf{J}}^*$  given by

$$\hat{\mathbf{J}}^* = \mathbf{J}^* + \tau_K(U^* - \hat{U}^*)\mathbf{n}.$$

Proposition 3 shows that the above problem admits a unique solution. Thanks to the  $O(h^{k+1})$  rate of convergence for both  $\mathbf{J}_{div}$  and  $\nabla \cdot \mathbf{J}_{div}$ , and to the super-convergence property for the local average of  $U$ , in [11, 14] the authors show that, for  $k \geq 1$ , the postprocessing approximation  $U^*$  converges with rate  $O(h^{k+2})$  in the  $L^2(\Omega)$  sense. This convergence behavior is confirmed numerically also for W-HDG in Section 6.

## 6 Numerical illustration

In this section, we will present some numerical experiments to verify the stability and convergence of our proposed numerical scheme. Before presenting the examples, we introduce a Gaussian quadrature rule to compute the inner-products  $(v, w)_{K, \mu_K}$  and  $\langle v, w \rangle_{\partial K, \mu_K}$  exactly when the element  $K = \Pi_{i=1}^d(a_i, b_i)$  is a hyperrectangle. The finite element space are defined using bi-polynomials, and  $\beta$  is a piecewise constant function. The weight function  $\mu$  is defined in accordance with (10) with  $\mathbf{x}_K$  denoting the center of  $K \in \mathcal{T}$ .

### 6.1 Quadrature schemes on rectangle elements with constant $\beta$

We first consider the one-dimensional case  $(v, w)_{\hat{K}, \mu}$  where  $\hat{K} = (0, 1)$  and  $\mu(\hat{x}) = \exp(-\hat{\beta}(\hat{x} - \hat{x}_{\hat{K}}))$  for some constant  $\hat{\beta}$ . We generate a Gaussian quadrature scheme  $\hat{Q}(\hat{\beta}, \hat{K})$  based on orthogonal polynomials up to degree  $k_0$  with respect to the inner-product  $(v, w)_{\hat{K}, \mu}$ . Our integral computation is exact when  $vw$  is a polynomial with degree at most  $2k_0 - 1$ . For any interval  $K = (a, b)$ , we can compute the inner-product by the change of variable  $x = a + h_K \hat{x}$  with  $h_K = b - a$ . Whence,

$$\int_K e^{-\beta(x - x_K)} v(x) w(x) dx = h_K \int_{\hat{K}} e^{-\beta h_K (\hat{x} - \hat{x}_{\hat{K}})} \hat{u} \hat{v} d\hat{x}.$$

The integral on the right hand side is computed exactly by the quadrature  $\widehat{Q}(h_K\beta, K)$ . For the multidimensional case with a constant  $\beta$ , we apply the tensor product quadrature rule to compute  $(v, w)_{K,\mu}$  based on the 1d quadrature scheme. Denoting the corresponding quadrature by  $Q_d(\beta, K)$  and given a face  $e$  of the element  $K$ , we note that we can compute similarly  $(v, w)_{e,\mu}$  by  $Q_{d-1}(\beta, e) \exp(-\beta \cdot (\mathbf{x}_e - \mathbf{x}_K))$ , with  $\mathbf{x}_e$  denoting the center of the face.

## 6.2 2D convergence tests on uniform Cartesian grids

We test our proposed numerical scheme (16) to approximate the problem (1) on the unit square  $\Omega = (0, 1)^2$ . Given a constant vector  $\beta = (\beta_1, \beta_2)^T$ , we define the analytic solution to be

$$u(x_1, x_2) = x_1 x_2 \frac{(1 - \exp((x_1 - 1)\beta_1))(1 - \exp((x_2 - 1)\beta_2))}{(1 - \exp(-\beta_1))(1 - \exp(-\beta_2))}$$

so that the solution vanishes at the boundary (as in the 1d case) and produces boundary layers along  $x_1 = 1$  and  $x_2 = 1$  when  $\beta_1$  and  $\beta_2$  are large enough, respectively.

### 6.2.1 Convergence for $(\mathbf{J}, U)$

Our numerical implementation relies on the `deal.II` finite element library [3] using bi-polynomial elements  $\mathcal{Q}_k$  under a sequence of quadrilateral subdivisions. Here we set  $\{\mathcal{T}_j\}_{j=1}^6$  to be sequence of uniform Cartesian grids with the mesh size  $h_j = 2^{-j-1}\sqrt{2}$ . In Table 1, we report the  $L^2(\Omega)$ -errors between  $(\mathbf{j}, u)$  and  $(\mathbf{J}, U)$  as well as the  $L^\infty(\Omega)$  errors for  $U$  using different degrees of bi-polynomials. We note that the stabilization parameter  $\tau$  is fixed to be 1 on all edges. The convergence rate showing in the table is computed with

$$\text{rate}_{j+1} := \log(e_{j+1}/e_j) / \log(\#\text{DoF}_{j+1}/\#\text{DoF}_j), \quad (34)$$

From Table 1, we observed optimal rate of convergence  $O(h^{k+1})$  in both  $L^2(\Omega)$  and  $L^\infty(\Omega)$  norms. Here we note that the  $L^\infty(\Omega)$ -error is approximated by comparing the values on the 6th-order Gaussian quadrature points on each cell. We also report the error behavior of the cell-wise average of  $U$ . That is  $\max_{K \in \mathcal{T}} (1, u - U)_K$ . We observe that this quantity superconverges with rate  $O(h^{2k+1})$  when  $k \geq 1$ . This will help us to obtain higher order rate of convergence in the procedure of the postprocessing using bi-polynomials  $\mathcal{Q}_{k+1}$ .

### 6.2.2 Convergence for the local postprocessing

We next examine the convergence of the local postprocessing  $U_*$  according to (31), i.e. reconstruction by the local  $L^2$  minimization. Table 2 reports the error decays for  $U_*$  in both  $L^2(\Omega)$  and  $L^\infty(\Omega)$  norms. Both errors decay with rate  $O(h^{k+2})$  for  $k \geq 1$ .



| deg | # cells | # DoFs  | $\ \mathbf{j} - \mathbf{J}\ _{L^2(\Omega)}$ |      | $\ u - U\ _{L^2(\Omega)}$ |       | $\ u - U\ _{L^\infty(\Omega)}$ |       | avg       |       |
|-----|---------|---------|---|------|---------------------------|-------|--------------------------------|-------|-----------|-------|
|     |         |         | error                                       | rate | error                     | rate  | error                          | rate  | error     | rate  |
| 0   | 16      | 48      | 8.186e+00                                   | -    | 2.583e-01                 | -     | 6.846e-01                      | -     | 4.024e-01 | -     |
|     | 64      | 192     | 5.679e+00                                   | 0.53 | 3.371e-01                 | -0.38 | 1.035e+00                      | -0.60 | 7.088e-01 | -0.82 |
|     | 256     | 768     | 3.402e+00                                   | 0.74 | 2.763e-01                 | 0.29  | 8.435e-01                      | 0.30  | 6.070e-01 | 0.22  |
|     | 1024    | 3072    | 2.115e+00                                   | 0.69 | 1.653e-01                 | 0.74  | 5.761e-01                      | 0.55  | 3.961e-01 | 0.62  |
|     | 4096    | 12288   | 1.363e+00                                   | 0.63 | 8.714e-02                 | 0.92  | 3.479e-01                      | 0.73  | 2.414e-01 | 0.71  |
|     | 16384   | 49152   | 8.366e-01                                   | 0.70 | 4.436e-02                 | 0.97  | 1.965e-01                      | 0.82  | 1.384e-01 | 0.80  |
|     | 65536   | 196608  | 4.775e-01                                   | 0.81 | 2.237e-02                 | 0.99  | 1.053e-01                      | 0.90  | 7.503e-02 | 0.88  |
| 1   | 16      | 192     | 2.218e+00                                   | -    | 9.313e-02                 | -     | 5.659e-01                      | -     | 1.706e-01 | -     |
|     | 64      | 768     | 1.107e+00                                   | 1.00 | 4.298e-02                 | 1.12  | 2.630e-01                      | 1.11  | 8.488e-02 | 1.01  |
|     | 256     | 3072    | 3.637e-01                                   | 1.61 | 1.403e-02                 | 1.62  | 1.163e-01                      | 1.18  | 1.860e-02 | 2.19  |
|     | 1024    | 12288   | 9.950e-02                                   | 1.87 | 3.842e-03                 | 1.87  | 3.887e-02                      | 1.58  | 3.460e-03 | 2.43  |
|     | 4096    | 49152   | 2.557e-02                                   | 1.96 | 9.880e-04                 | 1.96  | 1.120e-02                      | 1.80  | 5.357e-04 | 2.69  |
|     | 16384   | 196608  | 6.448e-03                                   | 1.99 | 2.493e-04                 | 1.99  | 2.999e-03                      | 1.90  | 7.450e-05 | 2.85  |
|     | 65536   | 786432  | 1.617e-03                                   | 2.00 | 6.252e-05                 | 2.00  | 7.756e-04                      | 1.95  | 9.821e-06 | 2.92  |
| 2   | 16      | 432     | 1.419e+00                                   | -    | 5.574e-02                 | -     | 2.518e-01                      | -     | 7.054e-02 | -     |
|     | 64      | 1728    | 3.199e-01                                   | 2.15 | 1.234e-02                 | 2.18  | 5.277e-02                      | 2.25  | 9.511e-03 | 2.89  |
|     | 256     | 6912    | 4.996e-02                                   | 2.68 | 1.929e-03                 | 2.68  | 8.822e-03                      | 2.58  | 5.021e-04 | 4.24  |
|     | 1024    | 27648   | 6.630e-03                                   | 2.91 | 2.562e-04                 | 2.91  | 1.239e-03                      | 2.83  | 2.195e-05 | 4.52  |
|     | 4096    | 110592  | 8.354e-04                                   | 2.99 | 3.229e-05                 | 2.99  | 1.765e-04                      | 2.81  | 8.334e-07 | 4.72  |
|     | 16384   | 442368  | 1.042e-04                                   | 3.00 | 4.028e-06                 | 3.00  | 2.395e-05                      | 2.88  | 2.874e-08 | 4.86  |
|     | 65536   | 1769472 | 1.299e-05                                   | 3.00 | 5.022e-07                 | 3.00  | 3.119e-06                      | 2.94  | 9.433e-10 | 4.93  |

Table 1: Errors and observed convergence rates between the fluxes  $\mathbf{j}$  and  $\mathbf{J}$  in  $L^2(\Omega)$  norm and between the densities  $u$  and  $U$  in both  $L^2(\Omega)$  and  $L^\infty(\Omega)$  norms using bi-polynomials  $\mathcal{Q}_k$  with  $k = 0, 1, 2$  under a sequence of uniform quadrilateral subdivisions. Optimal rates of convergences are observed. The last column shows the error decay for the cell-wise average of  $U$ , i.e.,  $\text{avg} := \max_{K \in \mathcal{T}} |(u - U)_K|$ .

| deg | # cells | # dofs  | $\ u - U_*\ _{L^2(\Omega)}$ |      | $\ u - U_*\ _{L^\infty(\Omega)}$ |      |
|-----|---------|---------|-----------------------------|------|----------------------------------|------|
|     |         |         | error                       | rate | error                            | rate |
| 1   | 16      | 192     | 7.868e-02                   | -    | 5.873e-01                        | -    |
|     | 64      | 768     | 2.309e-02                   | 1.77 | 2.566e-01                        | 1.19 |
|     | 256     | 3072    | 4.557e-03                   | 2.34 | 6.750e-02                        | 1.93 |
|     | 1024    | 12288   | 7.049e-04                   | 2.69 | 1.255e-02                        | 2.43 |
|     | 4096    | 49152   | 9.673e-05                   | 2.87 | 2.092e-03                        | 2.58 |
|     | 16384   | 196608  | 1.260e-05                   | 2.94 | 3.007e-04                        | 2.80 |
|     | 65536   | 786432  | 1.606e-06                   | 2.97 | 4.035e-05                        | 2.90 |
| 2   | 16      | 432     | 3.211e-02                   | -    | 2.485e-01                        | -    |
|     | 64      | 1728    | 3.985e-03                   | 3.01 | 5.269e-02                        | 2.24 |
|     | 256     | 6912    | 3.647e-04                   | 3.45 | 7.371e-03                        | 2.84 |
|     | 1024    | 27648   | 2.624e-05                   | 3.80 | 5.929e-04                        | 3.64 |
|     | 4096    | 110592  | 1.712e-06                   | 3.94 | 3.964e-05                        | 3.90 |
|     | 16384   | 442368  | 1.085e-07                   | 3.98 | 2.511e-06                        | 3.98 |
|     | 65536   | 1769472 | 6.813e-09                   | 3.99 | 1.574e-07                        | 4.00 |

Table 2: Error between the postprocess solution  $U_*$  ( $L^2$ -minimization) defined by (31) and the exact solution  $u$  in both  $L^2(\Omega)$  and  $L^\infty(\Omega)$  norms using bi-polynomials with degree 1 and 2. Optimal rates of convergence are observed.

Table 3 provides the convergence results for the flux reconstruction  $\mathbf{J}_{div}$  defined by (32) as well as the local postprocessing  $U^*$  based on  $\mathbf{J}_{div}$ ; see (33). We confirm numerically that both  $\mathbf{J}_{div}$  and  $\nabla \cdot \mathbf{J}_{div}$  converge with rate  $O(h^{k+1})$ . Such results, together with the superconvergence of the cell-wise average of  $U$  (see the last column of Table 1), guarantee that  $\|u - U^*\|_{L^2(\Omega)}$  decays with rate  $O(h^{k+2})$  and that the errors are greater than  $\|u - U_*\|_{L^2(\Omega)}$ . We also observe optimal convergence of  $U^*$  in  $L^\infty(\Omega)$ , with an error larger than the  $L^\infty(\Omega)$  error for  $U_*$ .

| deg | # cells | # DoFs  | $\ \mathbf{j} - \mathbf{J}_{div}\ _{L^2(\Omega)}$ |      | $\ \nabla \cdot \mathbf{j} - \nabla \cdot \mathbf{J}_{div}\ _{L^2(\Omega)}$ |      | $\ u - U^*\ _{L^2(\Omega)}$ |      | $\ u - U^*\ _{L^\infty(\Omega)}$ |      |
|-----|---------|---------|---|------|---|------|-----------------------------|------|----------------------------------|------|
|     |         |         | error   | rate | error   | rate | error                       | rate | error                            | rate |
| 1   | 16      | 192     | 2.259e+00   | -    | 4.4415e+00  | -    | 8.8866e-02                  | -    | 6.1846e-01                       | -    |
|     | 64      | 768     | 1.108e+00   | 1.03 | 2.2154e+00  | 1.00 | 3.0418e-02                  | 1.55 | 3.8536e-01                       | 0.68 |
|     | 256     | 3072    | 3.635e-01   | 1.61 | 6.9941e-01  | 1.66 | 6.2003e-03                  | 2.29 | 1.6328e-01                       | 1.24 |
|     | 1024    | 12288   | 9.942e-02   | 1.87 | 1.8539e-01  | 1.92 | 9.2468e-04                  | 2.75 | 3.3066e-02                       | 2.30 |
|     | 4096    | 49152   | 2.555e-02   | 1.96 | 4.6504e-02  | 2.00 | 1.2232e-04                  | 2.92 | 5.0770e-03                       | 2.70 |
|     | 16384   | 196608  | 6.443e-03   | 1.99 | 1.1557e-02  | 2.01 | 1.5584e-05                  | 2.97 | 6.9794e-04                       | 2.86 |
|     | 65536   | 786432  | 1.616e-03   | 2.00 | 2.8750e-03  | 2.01 | 1.9622e-06                  | 2.99 | 9.1424e-05                       | 2.93 |
| 2   | 16      | 432     | 1.419e+00   | -    | 3.5109e+00  | -    | 4.6873e-02                  | -    | 3.9884e-01                       | -    |
|     | 64      | 1728    | 3.197e-01   | 2.15 | 8.2793e-01  | 2.08 | 7.1029e-03                  | 2.72 | 2.3068e-01                       | 0.79 |
|     | 256     | 6912    | 4.992e-02   | 2.68 | 1.3070e-01  | 2.66 | 5.9918e-04                  | 3.57 | 2.7253e-02                       | 3.08 |
|     | 1024    | 27648   | 6.624e-03   | 2.91 | 1.7086e-02  | 2.94 | 4.0934e-05                  | 3.87 | 2.1080e-03                       | 3.69 |
|     | 4096    | 110592  | 8.347e-04   | 2.99 | 2.1204e-03  | 3.01 | 2.6252e-06                  | 3.96 | 1.4343e-04                       | 3.88 |
|     | 16384   | 442368  | 1.041e-04   | 3.00 | 2.6186e-04  | 3.02 | 1.6532e-07                  | 3.99 | 9.3157e-06                       | 3.94 |
|     | 65536   | 1769472 | 1.298e-05   | 3.00 | 3.2583e-05  | 3.01 | 1.1081e-08                  | 3.90 | 5.9344e-07                       | 3.97 |

Table 3:  $L^2(\Omega)$ -error decay for the flux reconstruction  $\mathbf{J}_{div}$  (defined by (32)) as well as its divergence. The  $L^2(\Omega)$  and  $L^\infty(\Omega)$  errors for the postprocessing  $U^*$  defined by (33) (based on flux reconstruction) are report in this table as well.

Figure 1 reports the approximate solution  $U$  and its postprocessing results  $U_*$  and  $U^*$  on the uniform grid  $\mathcal{T}_6$  (16384 cells). We observe that the error of  $U$  mainly concentrates on the two boundary layer but not on the top right corner of the domain. On the other hand, both  $U_*$  and  $U^*$  have large errors around the top-right corner. Meanwhile, cells near the two boundary layers contains both positive and negative errors, which behave differently compared to the error of  $U$ .

### 6.3 A one dimensional benchmark test

In section 4.8, we have pointed out that the Scharfetter–Gummel scheme (30) can be obtained as a certain limit of our proposed method. Here we perform a comparison test using these two numerical approaches as well as the standard HDG scheme to solve the stationary van Roosbroeck model in a one-dimensional domain  $\Omega = [0, \ell]$ .

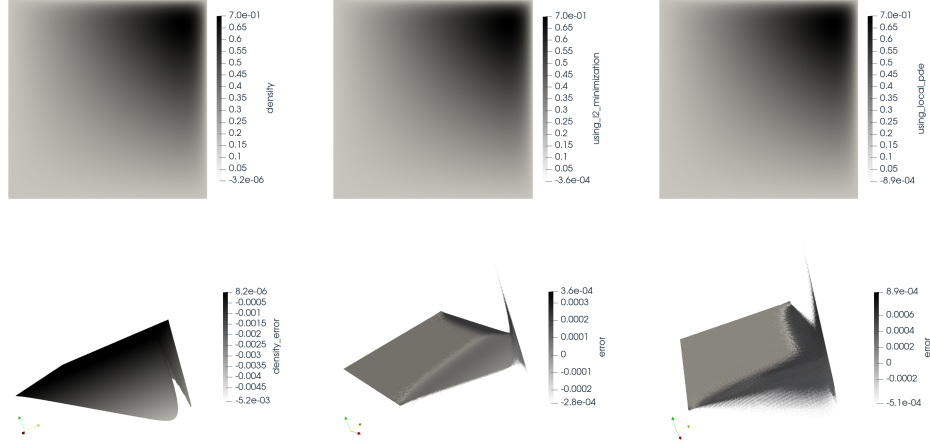


Figure 1: From left to right: approximate solutions  $U$ ,  $U_*$  and  $U^*$  (top) defined on the grid  $\mathcal{T}_6$  using bi-linear elements and the corresponding error plots (bottom). The range of the plots are  $[-5.2e-3, 8.2e-6]$ ,  $[-2.8e-4, 3.6e-4]$  and  $[-5.1e-4, 8.9e-4]$ . Here we rescaled magnitudes with factors 100, 1500, and 1000 respectively.

### 6.3.1 The van Roosbroeck system

The van Roosbroeck system is one of the most common models used to describe currents of electric charge carriers inside a semiconductor device. It consists of three nonlinear differential equations for the unknown electrostatic potential  $\psi(x)$ , the density of electrons  $n$  and the density of holes  $p$ . A complete description of this model can be found in [24]. In the following numerical test, we compute the so-called thermodynamic equilibrium, a physical state defined by vanishing currents. In equilibrium, it is possible to decouple the above mentioned three equations, i.e., solving a nonlinear Poisson equation to obtain  $\psi(x)$  and using this function to compute the other two unknown densities  $(n, p)$ .

Here the one dimensional Poisson equation for  $\psi(x)$  is given by

$$-\frac{d}{dx} \left( \varepsilon_s \frac{d}{dx} \psi \right) = q \left( N_v \exp \left( \frac{E_v - q\psi}{k_B T} \right) - N_c \exp \left( \frac{q\psi - E_c}{k_B T} \right) + C \right), \quad (35)$$

where  $q$  is the elementary charge,  $k_B$  is the Boltzmann constant,  $T$  represents the temperature of the device (which we will suppose to be constant on all  $\Omega$ ), and  $\varepsilon_s$ ,  $N_v$ ,  $E_v$ ,  $N_c$ ,  $E_c$ , and  $C$  are constants or piecewise constant functions that describe some physical properties of the material; we refer to Table 4 for all these values. Dirichlet boundary conditions for (35) can be obtained under the assumption that the right hand side datum vanishes at the boundary (cf. [24, Section 2.3]).

Given the electrostatic potential  $\psi$ , we shall solve  $n$  and  $p$  governed by a drift-diffusion system. Here we can solve them separately in thermal equilibrium and we only focus on the hole density. For the hole density, there holds

$$\begin{cases} -q \frac{d}{dx} \left( \mu_p \left( U_T \frac{dp}{dx} + p \frac{d\psi}{dx} \right) \right) = 0, \\ p(x_0) = N_v \exp \left( \frac{E_v - q\psi(x_0)}{k_B T} \right) \quad \text{for } x_0 \in \{0, \ell\}. \end{cases} \quad (36)$$

where  $U_T := \frac{k_B T}{q}$  and the mobility constant  $\mu_p$  defines how easy is for the holes to travel through the device. Comparing the above equation with (1), we have

$$\alpha := U_T, \quad \beta := -\frac{d\psi}{dx}, \quad f := 0.$$

### 6.3.2 Numerical settings

We will test our numerical method for (36) using the electrostatic potential given by (35). Here we consider our physical domain as a p-i-n device, which contains a  $p$ - and an  $n$ -doped regions as well as an intrinsic layer in between. The doping concentration  $C$  in (35) is assumed to be a piecewise constant function

$$C = \begin{cases} N_D, & \text{if } 0 \leq x < \frac{\ell}{3}, \\ 0, & \text{if } \frac{\ell}{3} \leq x < \frac{2\ell}{3}, \\ -N_A, & \text{if } x \geq \frac{2\ell}{3}, \end{cases} \quad (37)$$

where  $N_D$  and  $N_A$  are positive constants defined in Table 4. A graphical representation of the solutions to this problem is shown in Figure 2.

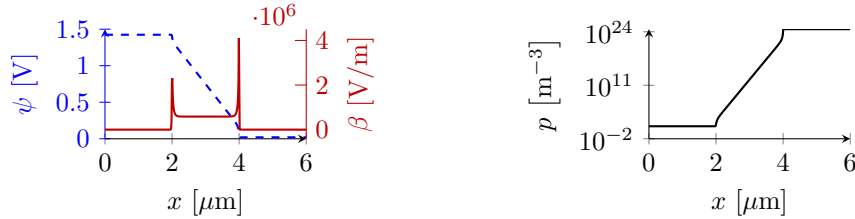


Figure 2: (Left) electrostatic potential  $\psi$  (dashed blue line) for (35) and the electric field  $\beta = -d\psi/dx$  (solid red line) for a model that uses the constants described in Table 4. (Right) the hole concentration for (36). Here we obtain the results using linear elements on a highly refined grid with 18432 cells and 92161 degrees of freedom (counting the degrees of freedom for the solution, its gradient and the solution on the trace).

We construct a sequence of hierarchical grids  $\{\mathcal{T}_i\}_i$  of  $\Omega$  for  $i$  in  $\{1, \dots, 7\}$ . The coarsest grid  $\mathcal{T}_1$  is a refinement of the uniform partition of  $\Omega$  with intervals

$I_j := (\frac{(j-1)\ell}{6}, \frac{j\ell}{6})$  for  $j = 1, \dots, 6$ , such that the two junctions  $\{\frac{\ell}{3}, \frac{2\ell}{3}\}$  are grid points of  $\mathcal{T}_i$ . Then we build  $\mathcal{T}_1$  as follows:

1. We set  $I_1, I_6 \in \mathcal{T}_1$ .
2. Bisect the rest of the intervals with the following graded strategy: for each  $I_j$  with  $j = 2, 3, 4, 5$ , we consider an affine transformation  $\mathcal{F}_j : I_j \rightarrow (0, 1)$  such the junction point is at 0. Then we subdivide  $(0, 1)$  uniformly with four intervals and rescale them by taking the square of the position, i.e., for  $i = 1$  the partition is given by  $\mathcal{P} := \{(\frac{(k-1)^2}{2^{i+2}}, \frac{k^2}{2^{i+2}})\}_{k=1}^{2^{i+1}}$ .
3.  $\mathcal{T}_1$  consists of  $I_1, I_6$ , and  $\mathcal{F}_j^{-1}(\mathcal{P})$  for  $j = 2, 3, 4, 5$ .

To generate  $\mathcal{T}_i$  for  $i > 1$ , we refine globally  $\{I_1, I_6\}$  with  $i$  times, and refine the other  $I_j$  intervals following Step 2. Examples of the grids in  $\{\mathcal{T}_i\}_{i=1}^3$  are shown in Figure 3.



Figure 3: The triangulation  $\mathcal{T}_j$  over  $\Omega$  with 18, 36 and 72 cells.

We approximate the solutions to (36) on  $\mathcal{T}_j$  with three different methods: the Scharfetter–Gummel scheme (30), the standard HDG method (H-LDG) [13] and our proposed one in (16). Denote the approximation of the hole density with  $P_j$ . We obtain a numerical reference solution  $P_r$  by solving the problem with the standard HDG method on a grid  $\mathcal{T}_r$  which is globally refined from  $\mathcal{T}_7$  four times. The coefficient  $\beta = -\frac{d\psi}{dx}$  is generated by solving the Poisson problem (35) on  $\mathcal{T}_r$  with the standard HDG and project (in the  $L^2$  sense) the resulting  $\beta$  onto  $\mathcal{Q}(\mathcal{T})$  using piecewise constant functions.

### 6.3.3 Results

In the top-left plot of Figure 4, we report the errors  $\|P_j - P_r\|_{L^2(\Omega)}$  versus the numbers of degrees of freedom, where, to maintain the comparison fair with the finite volume scheme, we use  $\mathcal{P}_0$  functions for the HDG and W-HDG approaches. It turns out that all three numerical methods converge to first order, however, the numerical solution computed using the standard HDG violates the maximum principle; see the top-right plot for the profile of  $P_4$ . On the other hand, the numerical results using (16) behaves similarly to the state-of-the-art solution obtained with Scharfetter–Gummel stabilized finite volumes.

It is common to postprocess the solution generated by the Scharfetter–Gummel stabilized finite volume scheme by connecting the mid-points of all

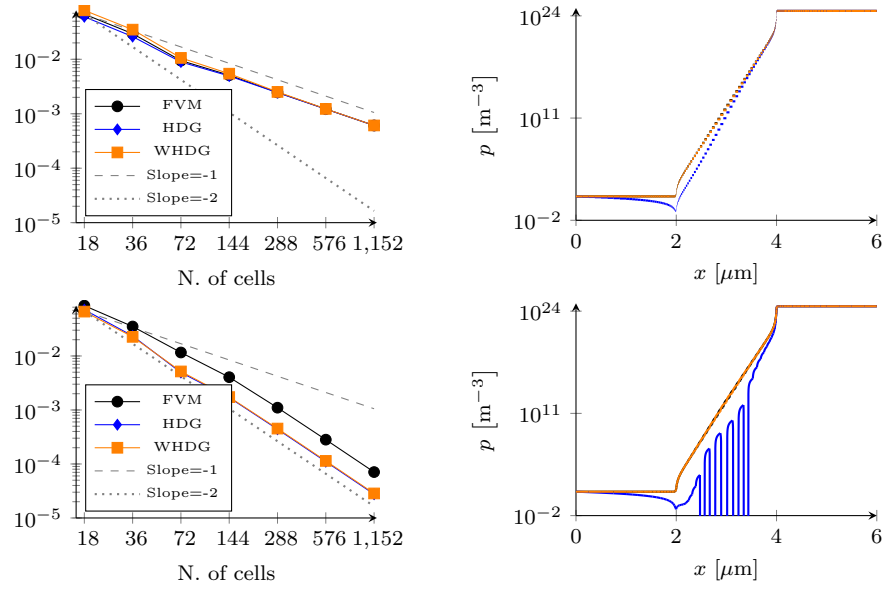


Figure 4: (Top-left)  $L^2(\Omega)$ -errors between  $P_j$  and  $P_r$  against the number cells using different numerical approaches. (Top-right) Numerical approximation of  $P_4$ . (Bottom-left) post-processing  $P_j^*$  of  $P_j$  using linear elements. (Bottom-right) Post-processing results for  $P_3^*$ . Here we have truncated the results  $P_3^*$  from the standard HDG for the values above  $10^{-2}\text{m}^{-3}$ .

| Physical Quantity           | Symbol          | Value                    | Units                                    |
|-----------------------------|-----------------|--------------------------|--|
| Device length               | $\ell$          | 6.00                     | $\mu\text{m}$                            |
| Reference temperature       | $T$             | 300                      | K  |
| Absolute permittivity       | $\varepsilon_s$ | $1.1422 \times 10^{-10}$ | $\text{F m}^{-1}$                        |
| Valence band density        | $N_v$           | $9.1396 \times 10^{24}$  | $\text{m}^{-3}$                          |
| Valence band-edge energy    | $E_v$           | 0                        | eV                                       |
| Conduction band density     | $N_c$           | $4.3520 \times 10^{23}$  | $\text{m}^{-3}$                          |
| Conduction band-edge energy | $E_c$           | 1.4240                   | eV                                       |
| Hole mobility               | $\mu_p$         | $4 \times 10^{-2}$       | $\text{m}^2 \text{V}^{-1} \text{s}^{-1}$ |
| Acceptor doping density     | $N_A$           | $4.2042 \times 10^{24}$  | $\text{m}^{-3}$                          |
| Donator doping density      | $N_D$           | $4.3520 \times 10^{23}$  | $\text{m}^{-3}$                          |
| Elementary charge           | $q$             | $1.6022 \times 10^{-19}$ | C  |
| Boltzmann constant          | $k_B$           | $1.3806 \times 10^{-23}$ | $\text{J K}^{-1}$                        |

Table 4: The physical constants used in Section 6.3.

cells with straight lines, obtaining a piecewise linear and continuous solution. Therefore, in the bottom part of Figure 4, we perform an analogous comparison after implementing this strategy for all three methods. In particular, for the HDG and W-HDG scheme, this algorithm has been implemented not by connecting the mid-points of the cells but the points on the trace obtained from  $\hat{u}$ . The bottom-left logarithmic plot shows that the resulting linear approximations, denoted by  $P_j^*$ , converge to  $P_r$  with second order in all cases. On the other side, the quality of the solution on the points where the charge carrier density is low (i.e., between 0 and  $\frac{2}{3}\ell$ ) is quite different between the FVM and W-HDG method and the standard HDG; indeed, the contribute of these regions on the global  $L^2$  error is negligible. On the bottom-right plot we can see the profile for  $P_3^*$ . The approximations from the FVM method and the W-HDG both satisfy the discrete maximum principle; instead, the result for the standard HDG method suffers the fact that some values of  $\hat{u}$  are negative (up to  $-2.284 \times 10^{13} \text{m}^{-3}$ ); therefore, here we only show the part with values above  $10^{-2} \text{m}^{-3}$ .

## 7 Conclusion

In this work we presented a weighted HDG method for the solution of convection-diffusion problems. The method is based on the introduction of weighted scalar products when defining the local HDG equations. The additional weights have the effect of a local Slotboom change of variable: they eliminate locally the drift term, transforming the local drift diffusion problems into diffusion problems with an exponential coefficient.

We prove well-posedness property of the method, validate its numerical stability as well as convergence properties, and provide a fair comparison with a state-of-the-art finite volume discretization using Scharfetter and Gummel stabilization, and with standard HDG methods, for a convection dominated problem with dramatic scale changes, derived from the modeling of a p-i-n semiconductor

junction.

W-HDG is equivalent to the Scharfetter and Gummel stabilized finite volume for piecewise constant polynomial approximations, and generalizes it to arbitrary high order, while maintaining similar stability properties. An important path of investigation would be the construction of a positivity preserving post-processing solution for W-HDG, which is not guaranteed from the current algorithm.

## References

- [1] Ali, G., Bartel, A., Günther, M., Tischendorf, C.: Elliptic partial differential-algebraic multiphysics models in electrical network design. *Mathematical Models and Methods in Applied Sciences* **13**(09), 1261–1278 (2003)
- [2] Ali, G., Rotundo, N.: An existence result for elliptic partial differential-algebraic equations arising in semiconductor modeling. *Nonlinear Analysis: Theory, Methods & Applications* **72**(12), 4666–4681 (2010)
- [3] Arndt, D., Bangerth, W., Blais, B., Fehling, M., Gassmöller, R., Heister, T., Heltai, L., Köcher, U., Kronbichler, M., Maier, M., Munch, P., Pelteret, J.P., Proell, S., Simon, K., Turcksin, B., Wells, D., Zhang, J.: The `deal.II` library, version 9.3. *Journal of Numerical Mathematics* **29**(3), 171–186 (2021, accepted for publication)
- [4] Arnold, D.N., Brezzi, F., Cockburn, B., Marini, L.D.: Unified analysis of discontinuous Galerkin methods for elliptic problems. *SIAM J. Numer. Anal.* **39**(5) (2001)
- [5] Bank, R.E., Rose, D.J.: Some error estimates for the box method. *SIAM J. Numer. Anal.* **24**, 777–787 (1987)
- [6] Bessemoulin-Chatard, M.: A finite volume scheme for convection–diffusion equations with nonlinear diffusion derived from the scharfetter–gummel scheme. *Numerische Mathematik* **121**(4), 637–670 (2012)
- [7] Brezzi, F., Fortin, M.: *Mixed and hybrid finite element methods*, vol. 15. Springer Science & Business Media (2012)
- [8] Brezzi, F., Marini, L.D., Pietra, P.: Numerical simulation of semiconductor devices. *Computer methods in applied mechanics and engineering* **75**(1-3), 493–514 (1989)
- [9] Brezzi, F., Marini, L.D., Pietra, P.: Two-dimensional exponential fitting and applications to drift-diffusion models. *SIAM Journal on Numerical Analysis* **26**(6), 1342–1355 (1989)



- [10] Chainais-Hillairet, C., Jüngel, A., Shpartko, P.: A finite-volume scheme for a spinorial matrix drift-diffusion model for semiconductors. *Numerical Methods for Partial Differential Equations* (2015)
- [11] Cockburn, B., Dong, B., Guzmán, J.: A superconvergent ldg-hybridizable galerkin method for second-order elliptic problems. *Mathematics of Computation* **77**(264), 1887–1916 (2008)
- [12] Cockburn, B., Dong, B., Guzmán, J., Restelli, M., Sacco, R.: A hybridizable discontinuous galerkin method for steady-state convection-diffusion-reaction problems. *SIAM Journal on Scientific Computing* **31**(5), 3827–3846 (2009)
- [13] Cockburn, B., Gopalakrishnan, J., Lazarov, R.: Unified hybridization of discontinuous galerkin, mixed, and continuous galerkin methods for second order elliptic problems. *SIAM Journal on Numerical Analysis* **47**(2), 1319–1365 (2009)
- [14] Cockburn, B., Guzmán, J., Wang, H.: Superconvergent discontinuous galerkin methods for second-order elliptic problems. *Mathematics of Computation* **78**(265), 1–24 (2009)
- [15] Ern, A., Guermond, J.L.: *Theory and practice of finite elements*, vol. 159. Springer (2004)
- [16] Farrell, P., Linke, A.: Uniform second order convergence of a complete flux scheme on unstructured 1d grids for a singularly perturbed advection–diffusion equation and some multidimensional extensions. *Journal of Scientific Computing* **72**(1), 373–395 (2017)
- [17] Farrell, P., Rotundo, N., Doan, D.H., Kantner, M., Fuhrmann, J., Koprucki, T.: Mathematical methods: Drift-diffusion models. In: J. Piprek (ed.) *Handbook of Optoelectronic Device Modeling and Simulation*, vol. 2, chap. 50, pp. 733–771. CRC Press (2017)
- [18] Gärtner, K.: Existence of bounded discrete steady state solutions of the van Roosbroeck system with monotone Fermi–Dirac statistic functions. *Journal of Computational Electronics* **14**(3), 773–787 (2015)
- [19] Grisvard, P.: *Elliptic problems in nonsmooth domains*. SIAM (2011)
- [20] van’t Hof, B., ten Thije Boonkamp, J.H.M., Mattheij, R.M.M.: Discretization of the stationary convection-diffusion-reaction equation. *Numer. Methods Partial Differential Equations* **14**(5), 607–625 (1998)
- [21] Lazarov, R.D., Zikatanov, L.T.: An exponential fitting scheme for general convection-diffusion equations on tetrahedral meshes. *arXiv preprint arXiv:1211.0869* (2012)

- [22] Liu, L., van Dijk, J., ten Thije Boonkkamp, J., Mihailova, D., van der Mullen, J.: The complete flux scheme—error analysis and application to plasma simulation. *Journal of Computational and Applied Mathematics* **250**(0), 229 – 243 (2013)
- [23] Markowich, P.A.: *The Stationary Semiconductor Device Equations*. Springer Vienna (1986)
- [24] Markowich, P.A.: *The Stationary Semiconductor Device Equations*. Springer-Verlag, Berlin, Heidelberg (1986)
- [25] Mock, M.S.: On equations describing steady-state carrier distributions in a semiconductor device. *Communications on Pure and Applied Mathematics* **25**(6), 781–792 (1972)
- [26] Morton, K.: *Numerical Solution Of Convection-Diffusion Problems*. Applied Mathematics. Taylor & Francis (1996)
- [27] Nguyen, N.C., Peraire, J., Cockburn, B.: An implicit high-order hybridizable discontinuous galerkin method for linear convection–diffusion equations. *Journal of Computational Physics* **228**(9), 3232–3254 (2009)
- [28] Roos, H.G., Stynes, M., Tobiska, L.: *Robust numerical methods for singularly perturbed differential equations*, *Springer Series in Computational Mathematics*, vol. 24, 2nd edn. Springer, Berlin (2008)
- [29] Scharfetter, D., Gummel, H.: Large-signal analysis of a silicon read diode oscillator. *IEEE Transactions on Electron Devices* **16**(1), 64–77 (1969)
- [30] Shewchuk, J.: Triangle: A two-dimensional quality mesh generator and Delaunay triangulator. <http://www.cs.cmu.edu/~quake/triangle.html>, University of California at Berkeley
- [31] Si, H.: Tetgen, a delaunay-based quality tetrahedral mesh generator. *ACM Trans. Math. Softw.* **41**(2), 11:1–11:36 (2015)
- [32] Taylor, M.E.: *Partial Differential Equations III*. Springer New York (2011)
- [33] Ten Thije Boonkkamp, J., Schilders, W.H.: An exponential fitting scheme for the electrothermal device equations specifically for the simulation of avalanche generation. *COMPEL-The international journal for computation and mathematics in electrical and electronic engineering* **12**(2), 95–111 (1993)
- [34] Thiart, G.D.: Improved finite-difference scheme for the solution of convection-diffusion problems with the simplen algorithm. *Numer. Heat Transfer, Part B* **18**(1), 81–95 (1990)
- [35] ten Thije Boonkkamp, J.: A complete flux scheme for one-dimensional combustion simulation. In: *Finite volumes for complex applications IV*, pp. 573–583. ISTE, London (2005)

- [36] ten Thije Boonkkamp, J., Anthonissen, M.: The finite volume-complete flux scheme for advection-diffusion-reaction equations. *Journal of Scientific Computing* **46**(1), 47–70 (2011)